



1 **Interannual snow accumulation variability on glaciers derived from repeat, spatially**
2 **extensive ground-penetrating radar surveys**

3
4 Daniel McGrath¹, Louis Sass², Shad O'Neel² Chris McNeil², Salvatore G. Candela³,
5 Emily H. Baker², and Hans-Peter Marshall⁴

6 ¹*Department of Geosciences, Colorado State University, Fort Collins, CO*

7 ²*U.S. Geological Survey Alaska Science Center, Anchorage, AK*

8 ³*School of Earth Sciences and Byrd Polar Research Center, Ohio State University,*
9 *Columbus, OH*

10 ⁴*Department of Geosciences, Boise State University, Boise, ID*

11 **Abstract**

12 There is significant uncertainty regarding the spatiotemporal distribution of seasonal
13 snow on glaciers, despite being a fundamental component of glacier mass balance. To
14 address this knowledge gap, we collected repeat, spatially extensive high-frequency
15 ground-penetrating radar (GPR) observations on two glaciers in Alaska for five
16 consecutive years. GPR measurements showed steep snow water equivalent (SWE)
17 elevation gradients at both sites; continental Gulkana Glacier's SWE gradient averaged
18 115 mm 100 m⁻¹ and maritime Wolverine Glacier's gradient averaged 440 mm 100 m⁻¹
19 (over >1000 m). We extrapolated GPR point observations across the glacier surface using
20 terrain parameters derived from digital elevation models as predictor variables in two
21 statistical models (stepwise multivariable linear regression and regression trees).
22 Elevation and proxies for wind redistribution had the greatest explanatory power, and
23 exhibited relatively time-constant coefficients over the study period. Both statistical
24 models yielded comparable estimates of glacier-wide average SWE (1 % average
25 difference at Gulkana, 4 % average difference at Wolverine), although the spatial
26 distributions produced by the models diverged in unsampled regions of the glacier,
27 particularly at Wolverine. In total, six different methods for estimating the glacier-wide
28 average agreed within ± 11 %. We assessed interannual variability in the spatial pattern
29 of snow accumulation predicted by the statistical models using two quantitative metrics.
30 Both glaciers exhibited a high degree of temporal stability, with ~85 % of the glacier area
31 experiencing less than 25 % normalized absolute variability over this five-year interval.
32 We found SWE at a sparse network (3 stakes per glacier) of long-term glaciological stake
33 sites to be highly correlated with the GPR-derived glacier-wide average. We estimate
34 that interannual variability in the spatial pattern of SWE is only a small component (4–10
35 % of glacier-wide average) of the total mass balance uncertainty and thus, our findings
36 support the concept that sparse stake networks effectively measure interannual variability



37 in winter balance on glaciers, rather than some spatially varying pattern of snow
38 accumulation.

39

40 **1. Introduction**

41 Our ability to quantify glacier mass balance is dependent on accurately resolving the
42 spatial and temporal distributions of snow accumulation and ablation. Significant
43 advances in our knowledge of ablation processes have improved observational and
44 modelling capacities (Hock, 2005; Huss and Hock, 2015; Fitzpatrick et al., 2017), yet
45 comparable advances in our understanding of the distribution of snow accumulation have
46 not kept pace (Hock et al., 2017). Reasons for this discrepancy are two-fold: (i) snow
47 accumulation exhibits higher variability than ablation, both in magnitude and length
48 scale, largely due to wind redistribution in the complex high-relief terrain where
49 mountain glaciers are typically found (Kuhn et al., 1995) and (ii) accumulation
50 observations are typically less representative (i.e., one stake in a few hundred meter
51 elevation band) or less effective than comparable ablation observations (i.e., precipitation
52 gage measuring snowfall vs. radiometer measuring short-wave radiation). This
53 discrepancy presents a significant limitation to process-based understanding of mass
54 balance drivers. Furthermore, a warming climate has already modified – and will
55 continue to modify – the magnitude and spatial distribution of snow on glaciers through a
56 reduction in the fraction of precipitation falling as snow and an increase in rain-on-snow
57 events (Knowles et al., 2006; McAfee et al., 2013; Klos et al., 2014; McGrath et al.,
58 2017; Littel et al., 2018).

59

60 Significant research has been conducted on the spatial and, to a lesser degree, the
61 temporal variability of seasonal snow in mountainous and high-latitude landscapes (e.g.,
62 Balk and Elder, 2000; Molotch et al., 2005; Erickson et al., 2005; Deems et al., 2008;
63 Sturm and Wagner, 2010; Schirmer et al., 2011; Winstral and Marks, 2014; Anderson et
64 al., 2014; Painter et al., 2016). Although major advances have occurred in applying
65 physically-based snow distribution models (i.e., iSnoPal (Marks et al., 1999), SnowModel
66 (Liston and Elder, 2006), Alpine 3D (Lehning et al., 2006)), the paucity of required
67 meteorological forcing data proximal to glaciers limits widespread application. Many
68 other studies have successfully developed statistical approaches that rely on the



69 relationship between the distribution of snow water equivalent (SWE) and physically-
70 based terrain parameters (also referred to as physiographic or topographic properties or
71 variables) to model the distribution of SWE across entire basins (e.g., Molotch et al.,
72 2005; Anderson et al., 2014; Sold et al., 2013; McGrath et al., 2015).
73
74 A major uncertainty identified by these studies is the degree to which these statistically
75 derived relationships remain stationary in time. Many studies (Erickson et al., 2005;
76 Deems et al., 2008; Sturm and Wagner, 2010; Schirmer et al., 2011; Winstral and Marks,
77 2014; Helfricht et al., 2014) have found ‘time-stability’ in the distribution of SWE,
78 including locations where wind redistribution is a major control on this distribution. For
79 instance, a climatological snow distribution pattern, produced from the mean of nine
80 standardized surveys, accurately predicted the observed snow depth in a subsequent
81 survey in a tundra basin in Alaska (~4–10 cm root mean square error; Sturm and Wagner,
82 2010). Repeat LiDAR surveys over two years at three hillslope-scale study plots in the
83 Swiss Alps found a high degree of correlation ($r=0.97$) in snow depth spatial patterns
84 (Schirmer et al., 2011). They found that the final snow depth distributions at the end of
85 the two winter seasons were more similar than the distributions of any two individual
86 storms during that two-year period (Schirmer et al., 2011). Lastly, an 11-year study of
87 extensive snow probing (~1200 point observations) at a 0.36 km² field site in
88 southwestern Idaho found consistent spatial patterns ($r=0.84$; Winstral and Marks, 2014).
89 Collectively, these studies suggest that in landscapes characterized by complex
90 topography and extensive wind redistribution of snow, spatial patterns are largely time-
91 stable or stationary, as long as the primary drivers are stationary.
92
93 Even fewer studies have examined the question of interannual variability in the context of
94 snow distribution on glaciers. One study of two successive end-of-winter surveys of snow
95 depth on a glacier in Svalbard found strong interannual variability in the spatial
96 distribution of snow, and the relationship between snow distribution and topographic
97 features (Hodgkins et al., 2006). Elevation was found to only explain 38–60 % of the
98 variability in snow depth, and in one year, snow depth was not dependent on elevation in
99 the accumulation zone (Hodgkins et al., 2006). Instead, aspect, reflecting relative



100 exposure or shelter from prevailing winds, was found to be a significant predictor of
101 accumulation patterns. Repeat airborne LiDAR surveys of a ~36 km² basin (~50% glacier
102 cover) in Austria over five winters found that the glacierized area exhibited less
103 interannual variability (as measured by the interannual standard deviation) than the non-
104 glacierized sectors of the basin (Helfricht et al., 2014). Similarly, a three-year study of
105 snow distribution on Findelgletscher in the Swiss Alps using ground-penetrating radar
106 (GPR) found low interannual variability, as 86 % of the glacier area experienced less than
107 25 % normalized relative variability (Sold et al., 2016). These latter studies suggest that
108 seasonal snow distribution on glaciers likely exhibits ‘time-stability’ in its distribution,
109 but few datasets exist to robustly test this hypothesis. The ‘time-stability’ of snow
110 distribution on glaciers has particularly important implications for long-term glacier mass
111 balance programs, as annual mass balance solutions are derived from the integration of a
112 limited number of point observations (e.g., 3 to 15 stakes), and the assumption that stake
113 and snow pit observations accurately represent interannual variability in mass balance
114 rather than interannual variability in the spatial patterns of mass balance. Accurately
115 quantifying the magnitude and spatial distribution of glacier seasonal mass balances is a
116 prerequisite for understanding the water budget of glacierized basins, with direct
117 implications for any potential use of this water, whether that be ecological, agricultural,
118 or human consumption (Kaser et al., 2010).

119
120 To better understand the ‘time-stability’ of the spatial pattern of snow accumulation on
121 glaciers, we present five consecutive years of extensive GPR observations for two
122 glaciers in Alaska. First, we use these GPR-derived SWE measurements to train two
123 different types of statistical models, which were subsequently used to spatially
124 extrapolate SWE across each glacier’s area. Second, we assess the temporal stability in
125 the resulting spatial distribution in SWE. Finally, we compare GPR-derived winter mass
126 balance estimates to traditional glaciological derived mass balance estimates and quantify
127 the uncertainty that interannual variability in spatial patterns in snow accumulation
128 introduces to these estimates.

129

130 2. Study Area



131 During the spring seasons of 2013–2017, we conducted GPR surveys on Wolverine and
132 Gulkana glaciers, located on the Kenai Peninsula and eastern Alaskan Range in Alaska
133 (Fig. 1). These glaciers have been studied as part of the U.S. Geological Survey’s
134 Benchmark Glacier project since 1966 (O’Neel et al., 2014). Both glaciers are ~16 km² in
135 area and span ~1200 m in elevation. Wolverine Glacier exists in a maritime climate,
136 characterized by warm air temperatures (mean annual temperature = -0.2 °C at 990
137 meters) and high precipitation (median glacier-wide winter balance = 2.0 m water
138 equivalent (m w.e.)), while Gulkana is located in a continental climate, characterized by
139 colder air temperatures (mean annual temperature = -2.8 °C at 1480 meters) and low
140 precipitation (median glacier-wide winter balance = 1.2 m w.e.) (Fig. 2). The cumulative
141 mass balance time series for both glaciers is negative (~ -24 m w.e. between 1966–2016),
142 with Gulkana showing a more monotonic decrease over the entire study interval, while
143 Wolverine exhibited near equilibrium balance between 1966 and 1987, and sharply
144 negative to present (O’Neel et al., 2014; O’Neel et al., 2018).

145

146 **3. Methods**

147 The primary SWE observations are derived from a GPR measurement of two-way travel
148 time (*twt*) through the annual snow accumulation layer. We describe five main steps to
149 convert *twt* along the survey profiles to annual distributed SWE products for each glacier.
150 These include (i) acquisition of GPR and ground-truth data, (ii) calculation of snow
151 density and associated radar velocity, which are used to convert measured *twt* to annual
152 layer depth and subsequently SWE, and (iii) application of terrain parameter statistical
153 models to extrapolate SWE across the glacier area. We then describe approaches to (iv)
154 evaluate the temporal consistency in spatial SWE patterns and (v) compare GPR-derived
155 SWE and direct (glaciological) winter mass balances.

156

157 **3.1. Radar data collection and processing**

158 Common-offset GPR surveys were conducted with a 500 MHz Sensors and Software
159 Pulse Ekko Pro system in late spring close to maximum end-of-winter SWE and prior to
160 the onset of extensive surface melt. GPR parameters were set to a waveform-sampling
161 rate of 0.1 ns, a 200-ns time window, and “Free Run” trace increments, where samples



162 are collected as fast as the processor allows, instead of at uniform temporal or spatial
163 increments.

164

165 In general, GPR surveys were conducted by mounting a plastic sled behind a snowmobile
166 and driving at a near-constant velocity of 15 km h⁻¹ (Fig. 3, S1, S2), resulting in a trace
167 spacing of ~20 cm. Coincident GPS data were collected using a Novatel Smart-V1 GPS
168 receiver (Omnistar corrected, L1 receiver with root-mean-square accuracy of 0.9 m
169 (Perez-Ruiz et al., 2011)). We collected a consistent survey track from year-to-year that
170 minimized safety hazards (crevasses, avalanche runouts) but optimized the sampling of
171 terrain parameter space on the glacier (e.g., range and distribution of elevation, slope,
172 aspect, curvature, etc.). However, in 2016 at Wolverine Glacier, weather conditions and
173 logistics did not allow for ground surveys to be completed. Instead, a number of radar
174 lines were collected via a helicopter survey. To best approximate the ground surveys
175 completed in other years, we selected a subset of helicopter GPR observations within 150
176 m of the ground-based surveys. Previous comparisons between ground and helicopter
177 platforms found excellent agreement in SWE point observations ($r^2=0.96$, root mean
178 square error=0.14 m; McGrath et al., 2015).

179

180 Radargrams were processed using the ReflexW-2D software package (Sandmeier
181 Scientific Software). All radargrams were corrected to time zero, taken as the first
182 negative peak in the direct wave (Yelf and Yelf, 2006), and a dewow filter (mean
183 subtraction) was applied over 2 ns. When reflectors from the base of the seasonal snow
184 cover were insufficiently resolved, gain and band-pass filters were subsequently applied.
185 Layer picking was guided by ground-truth efforts but done semi-automatically using a
186 phase-following layer picker. For further details, please see McGrath et al. (2015).

187

188 **3.2. Ground truth observations**

189 We collected extensive ground-truth data to validate GPR surveys, including probing and
190 snowpit/cores. In the ablation zone of each glacier, we probed the snowpack thickness
191 every ~500 m along-track. In addition, we measured seasonal snow depth and density at
192 four locations (corresponding to the glaciological observations; see Section 3.5) on each



193 glacier in each year. We measured snow density using a gravimetric approach at 10–40
194 cm intervals in each snowpit, and along 7.25 cm diameter cores (if total depth >2 m) to
195 the summer surface. We calculated a density profile and column-average density, ρ_{site} , at
196 each site.

197

198 As snow densities did not exhibit a consistent spatial nor elevation dependency on the
199 glaciers, we calculated a single average density, ρ , of all ρ_{site} on each glacier and each
200 year, which was subsequently used to calculate SWE:

201

$$202 \quad SWE = \left(\frac{twt}{2}\right) \cdot v_s \cdot \rho. \quad (1)$$

203

204 where twt is the two-way travel time as measured by the GPR and v_s is the radar
205 velocity. v_s was calculated for each glacier in each year as the average of two
206 independent approaches: (i) an empirical relationship based on the glacier-wide average ρ
207 (Kovacs et al., 1995) and (ii) a least-squares regression between snow depth derived by
208 probing and all radar twt observations within a 3-m radius of the probe site. An
209 exception was made at Wolverine in 2016 as no coincident probe depth observations
210 were made during the helicopter-based surveys. Instead, we estimated the second radar
211 velocity by averaging radar velocities calculated from observed twt and snow depths at
212 three snowpit/core locations.

213

214 **3.3. Spatial Extrapolation**

215 Extrapolating SWE from point measurements to the basin scale has been a topic of
216 focused research for decades (e.g., Woo and Marsh, 1978; Elder et al., 1995; Molotch et
217 al., 2005). Most commonly, the dependent variable SWE is related to a series of
218 explanatory terrain parameters, which are proxies for the physical processes that actually
219 control SWE distribution across the landscape. These include orographic gradient in
220 precipitation (elevation), wind redistribution of existing snow (slope, curvature, drift
221 potential), and aspect with respect to solar radiation and prevailing winds (eastness,
222 northness). We derived terrain parameters from 10-m resolution digital elevation models
223 (DEMs) sourced from the ArcticDEM project (Noh and Howat, 2015) for Gulkana and



224 produced from airborne Structure from Motion photogrammetry at Wolverine (Nolan et
225 al., 2015). Both DEMs were based on imagery from August 2015. Specifically, these
226 parameters include elevation, surface slope, surface curvature, northness (Molotch et al.,
227 2005), eastness, and snow drift potential (S_b) (Winstral et al., 2002; Winstral et al., 2013;
228 Fig. S3, S4). For S_b , we determined direction by calculating the modal daily wind
229 direction during the winter (October – May) when wind speeds exceeded 5 m s^{-1}
230 (~minimum wind velocity for snow transport; Li and Pomeroy, 1997), and the length
231 scales for curvature using an optimization scheme that identified the highest model r^2 .
232

233 Prior to spatial extrapolation, we aggregated GPR observations to the resolution of the
234 DEM by calculating the median value of all observations within each 10 m pixel of the
235 DEM. We then utilized two approaches to extrapolate GPR point observations across the
236 glacier surface: (i) least-squares elevation gradient applied to glacier hypsometry and (ii)
237 statistical models. For (i), we derived SWE elevation gradients in two ways; first, solely
238 on observations that followed the glacier centerline and second, from the entire spatially-
239 extensive dataset. For (ii), we utilized both stepwise multivariable linear regressions and
240 regression trees (Breiman et al., 1984). All of these approaches produced a spatially-
241 distributed SWE field over the entire glacier area. Individual points in this field are
242 equivalent to point winter balances (b_w ; m w.e.). From the distributed b_w field, we
243 calculated a mean area-averaged winter balance (B_w ; m w.e.).
244

245 Additionally, we implemented a cross-validation approach to the statistical extrapolations
246 (multivariable regression and regression tree), whereby 75 % of the aggregated
247 observations were used for training and 25 % were used for testing. However, rather than
248 randomly selecting pixels from across the entire dataset, we randomly selected a single
249 pixel containing aggregated GPR observations and then extended this selection out along
250 continuous survey lines until we reached 25 % of the total observational dataset, thus
251 removing entire sections (and respective terrain parameters) from the analysis (Fig. S5).
252 This approach provided a more realistic test for the statistical models, as the random
253 selection of individual cells did not significantly alter terrain-parameter distributions. For
254 each glacier and each year, we produced 100 training/test dataset combinations, but rather



255 than take the single model with the highest r^2 or lowest RMSE from the resulting test
256 dataset, we produced a distributed SWE product by taking the median value for each
257 pixel from all 100 model runs and a glacier-wide median value that is the median of all
258 100 individual Bw estimates. We chose the median-value approach over a highest
259 r^2 /lowest RMSE approach that is often utilized because, despite being randomly selected,
260 some training datasets were inherently advantaged by a more complete distribution of
261 terrain parameters. These iterations resulted in the highest r^2 /lowest RMSE when applied
262 to the training dataset, but weren't necessarily indicative of a better model.

263

264 3.3.2. Stepwise Multivariable Linear Regression

265 We used a stepwise multivariable linear regression model of the form,

$$266 SWE_{(i,j)} = c_1x_{1(i,j)} + c_2x_{2(i,j)} + \dots + c_nx_{n(i,j)} + \varepsilon_{(i,j)}, \quad (2)$$

267 where $SWE_{(i,j)}$ is the predicted (standardized) value at location i,j and c_1, c_2, c_n are the beta
268 coefficients of the model, x_1, x_2, x_n are terrain parameters which are independent variables
269 that have been standardized and ε is the residual. We applied the regression model
270 stepwise and included an independent variable if it minimized the Akaike information
271 criterion (AIC; Akaike, 1974). We present the beta coefficients from each regression
272 (each year, each glacier) to explore the temporal stability of these terms.

273

274 3.3.3. Regression Trees

275 Regression trees (Breiman et al., 1984) provide an alternative statistical approach for
276 extrapolating point observations by recursively partitioning SWE into progressively more
277 homogenous subsets based on independent terrain parameter predictors (Molotch et al.,
278 2005; Meromy et al., 2013; Bair et al., 2018). The primary advantage of the regression
279 tree approach over the previously described MVR model is that each terrain parameter is
280 used multiple times to partition the observations, thereby allowing for non-linear
281 interactions between these terms. In contrast, the MVR only allows for a single “global”
282 linear relationship for each parameter across the entire parameter-space. We implemented
283 a random forest approach (Breiman, 2001) of repeated regression trees (100 learning
284 cycles) in Matlab, using weak learners and bootstrap aggregating (bagging; Breiman,
285 1996). Each weak learner omits 37% of observations, such that these “out-of-bag”



286 observations are used to calculate predictor importance. The use of this ensemble/bagging
287 approach reduces overfitting and thus precludes having to subjectively prune the tree and
288 provides more accurate and unbiased error estimates (Breiman, 2001). Prior to
289 implementing the regression tree, we removed the SWE elevation gradient from the
290 observations using a least-squares regression. As described in the results, elevation is the
291 dominant independent variable and as our observations (particularly at Wolverine) did
292 not cover the entire elevation range, the regression tree approach was not well suited to
293 predicting SWE at elevations outside of the observational range.

294

295 **3.4. Interannual variability in spatial patterns**

296 We quantified the stability of spatial patterns in SWE across the five-year interval using
297 two approaches: (i) normalized range and (ii) the coefficient of determination. In the first
298 approach, we first divided each pixel in the distributed SWE fields by the glacier-wide
299 average, B_w , for each year and each glacier, and then calculated the range in these
300 normalized values over the entire five-year interval. For example, if a cell has normalized
301 values of 84 %, 92 %, 106 %, 112 % and 120 %, the normalized range would be 36 %. A
302 limitation of this approach is that it is highly sensitive to outliers, such that a single year
303 can substantially increase this range. This is similar to an approach presented by Sold et
304 al. (2016), but unlike their calculation (their Fig. 9), the normalized values reported here
305 have not been further normalized by the normalized mean of that pixel over the study
306 interval. Thus, the values reported here are an absolute normalized range, whereas Sold et
307 al. (2016) report a relative normalized range. In the coefficient of determination (r^2)
308 approach, we computed the least-squares regression correlation between the SWE in each
309 pixel and the glacier-wide average, B_w , derived from the MVR model over the five-year
310 period. For this approach, cells with a higher r^2 scale linearly with the glacier-wide
311 average, while those with low r^2 do not.

312

313 **3.5. Glaciological mass balance**

314 Glacier-wide seasonal (winter, B_w ; summer, B_s) and annual balances (B_a) have been derived
315 from sparse glaciological measurements, made at fixed locations of each glacier, since 1966.
316 Historically, the integration of these sparse point measurements was accomplished using a site-



317 index method – equivalent to an area-weighted average ((March and Trabant, 1996; van
318 Beusekom et al., 2010). Systematic bias in the glaciological mass balance time-series is
319 removed via a geodetic adjustment derived from DEM differencing over decadal timescales
320 (e.g., O’Neel et al., 2014). Glaciological measurements were made within a day of the GPR
321 surveys each year, and integrated over the glacier hypsometry using both the historically
322 applied site-index method (based on the long-term three stake network) and a more commonly
323 applied balance profile method (based on the more extensive stake network initiated in 2009)
324 (Cogley et al., 2011). We utilized a single glacier hypsometry, derived from the 2015 DEMs,
325 for each glacier over the entire five-year interval. In order to facilitate a more direct
326 comparison to the GPR-derived B_w estimates, we used glaciological B_w estimates that have not
327 been geodetically calibrated.

328

329 **4. Results**

330 **4.1. General accumulation conditions**

331 Since 1966, Wolverine Glacier’s median B_w exceeds Gulkana’s by more than a factor of
332 two (2.3 vs. 1.1 m w.e.), and exhibits greater variability, with an interquartile range more
333 than twice as large (0.95 m w.e. vs. 0.4 m w.e.). Over the five-year study period, both
334 glaciers experienced accumulation conditions that spanned their historical ranges, with
335 one year in the upper quartile (including the 5th greatest B_w at Wolverine in 2016), one
336 year within 25% of the median, and multiple years in the lower quartile (2017 at Gulkana
337 and 2014 at Wolverine had particularly low B_w values) (Fig. 2). In all years, B_w at
338 Wolverine was greater, although in 2013 and 2014, the difference was only 0.1 m w.e..

339

340 Average accumulation season (taken as October 1 – May 31) wind speeds over the study
341 period were stronger (~ 7 m s^{-1} vs. ~ 3 m s^{-1}) and from a more consistent direction at
342 Wolverine than Gulkana (northeast at Wolverine, southwest to northeast at Gulkana)
343 (Fig. S6). On average, Wolverine experienced ~ 50 days with wind gusts > 15 m s^{-1} each
344 winter, while for Gulkana, this only occurred on ~ 7 days. Over the five-year study period,
345 interannual variability in wind direction was very low at Wolverine (2016 saw slightly
346 greater variability, with an increase in easterly winds). In contrast, at Gulkana, winds



347 were primarily from the northeast to east in 2013–2015, from the southwest to south in
348 2016–2017, and experienced much greater variability during any single winter.

349

350 **4.2. *In situ* and GPR point observations**

351 Glacier-averaged snow densities across all years were 440 kg m^{-3} (range $414\text{--}456 \text{ kg m}^{-3}$)
352 at Wolverine and 362 kg m^{-3} (range $328\text{--}380 \text{ kg m}^{-3}$) at Gulkana (Table S1). Average
353 radar velocities were 0.218 m ns^{-1} (range $0.207\text{--}0.229 \text{ m ns}^{-1}$) at Wolverine and 0.223 m
354 ns^{-1} ($0.211\text{--}0.231 \text{ m ns}^{-1}$) at Gulkana. Over this five-year interval, the GPR point
355 observations revealed a general pattern of increasing SWE with elevation, along with
356 fine-scale variability due to wind redistribution (e.g., upper elevations of Wolverine) and
357 localized avalanche input (e.g., lower west branch of Gulkana) (Fig. S1, S2). The SWE
358 elevation gradient was steeper (~ 440 vs. $\sim 115 \text{ mm } 100 \text{ m}^{-1}$) and more variable in its
359 magnitude at Wolverine than Gulkana. Gradients ranged between $348 - 624 \text{ mm } 100 \text{ m}^{-1}$
360 at Wolverine, and $74 - 154 \text{ mm } 100 \text{ m}^{-1}$ at Gulkana (Fig. 4). Over all five years at both
361 glaciers, elevation explained between 50 % and 83 % of the observed variability in SWE
362 (Fig. 4).

363

364 **4.3. Model performance**

365 To evaluate model performance in unsampled locations of the glacier, both extrapolation
366 approaches were run 100 times for each glacier and each year, each time with a unique,
367 randomly selected training (75 % of aggregated observations) and test (remaining 25 %
368 of aggregated observations) dataset. The median and standard deviation of the
369 coefficients of determination (r^2) from these 100 models runs are shown in Fig. 5. Model
370 performance ranged from 0.25 to 0.75, but on average, across both glaciers and all years,
371 was 0.56 for the MVR approach and 0.46 for the regression tree. Model performance was
372 higher and more consistent at Wolverine, whereas 2015 and 2017 at Gulkana had test
373 dataset r^2 of ~ 0.4 and 0.3 , likely reflecting the lower SWE elevation gradients and
374 coefficients of determination with elevation during these years (Fig. 4). The wide range
375 in r^2 across the 100 model runs reflects the variability in training and test datasets that
376 were randomly selected. When the test dataset terrain parameter space was captured by
377 the training dataset, a high coefficient of determination resulted, but when the test dataset



378 terrain parameter space was exclusive , e.g., contained only a small elevation range, the
379 model performance was typically low. This further highlights the importance of elevation
380 as a predictor for these glaciers.

381

382 At Gulkana, the model residuals (Fig. S1) exhibited spatiotemporal consistency, with
383 positive residuals (i.e., observed SWE exceeded modeled SWE) at mid-elevations of the
384 west branch, and at the very terminus of the glacier. The largest negative residuals
385 typically occurred at the highest elevations. In both cases, these locations deviated from
386 the overall SWE elevation gradient. At Wolverine, observations at the highest elevations
387 typically exceeded the modeled SWE, particularly in the northeast quadrant of the glacier
388 (Fig. S2). Elsewhere at Wolverine, the residuals often alternated between positive and
389 negative values over length scales of 10s to 100s of meters (Fig. S2), which we interpret
390 as zones of scour/drift that were better captured by the regression tree models.

391

392 The beta coefficients of terrain parameters from the MVR were fairly consistent from
393 year-to-year at both glaciers (Fig. 6). At Wolverine, elevation was the largest beta
394 coefficient, followed by Sb and curvature. At Gulkana, elevation was also the largest beta
395 coefficient, followed by curvature. Gulkana experiences much greater variability in wind
396 direction during the winter months (Fig. S6), possibly explaining why Sb was either not
397 included or had a very low beta coefficient in the median regression model. As our
398 surveys were completed prior to the onset of ablation, terrain parameters related to solar
399 radiation gain (notably the terms that include aspect: northness and eastness) had small
400 and variable beta coefficients.

401

402 **4.4. Spatial Variability**

403 A common approach for quantifying snow accumulation variability across a range of
404 means is the coefficient of variation (CoV), calculated as the ratio of the standard
405 deviation to the mean (Liston et al., 2004; Winstral and Marks, 2014). The mean and
406 standard deviation of CoVs at Wolverine were 0.42 ± 0.03 and at Gulkana, 0.29 ± 0.05 ,
407 indicating relatively lower spatial variability in SWE at Gulkana (Fig. 7). CoVs were
408 fairly consistent across all five years, although 2017 saw the largest CoVs at both



409 glaciers. Interestingly, 2017 had the lowest absolute spatial variability (i.e., lowest
410 standard deviation), but also the lowest glacier-wide averages during the study period,
411 resulting in greater CoVs.
412
413 Qualitatively, both Wolverine and Gulkana glaciers exhibited consistent spatiotemporal
414 patterns in accumulation across the glacier surface, with elevation exerting a first-order
415 control (Fig. 8, S7, S8). Overlaid on the strong elevational gradient are consistent
416 locations of wind scour and deposition, reflecting the interaction of wind redistribution
417 and complex – albeit relatively stable year to year – surface topography (consisting of
418 both land and ice topography). For instance, numerous large drifts (~2 m amplitude, ~200
419 m wavelength) occupy the northeast corner of Wolverine Glacier, where prevailing
420 northeasterly winds consistently redistributed snow into sheltered locations in each year
421 of the study period (Fig. 8). The different statistical extrapolation approaches produced
422 nearly identical B_w estimates (4 % difference on average at Wolverine and 1 % difference
423 on average at Gulkana) (Fig. 9). The MVR B_w estimate was larger in 4 out of 5 years at
424 Wolverine (Fig. 9), while neither approach exhibited a consistent bias at Gulkana.
425
426 Although the glacier-wide averages between these approaches showed close agreement,
427 we explored the differences in spatial patterns by calculating a mean SWE difference
428 map for each glacier, by differencing the five-year mean SWE produced by the regression
429 tree model from the same produced by the MVR model (Fig. 10). As such, locations
430 where the MVR exceeded the regression tree are positive (yellow). At Gulkana, where
431 the two approaches showed slightly better glacier-wide B_w agreement, the magnitude in
432 individual pixel differences were substantially less than at Wolverine (e.g., color bar
433 scales range ± 0.2 m at Gulkana vs. ± 0.5 m at Wolverine). At Wolverine Glacier, there
434 were three distinct elevation bands where the MVR approach predicted greater SWE,
435 namely the main icefall in the ablation zone, a region of complex topography centered
436 around a normalized elevation of 0.65, and lastly, at higher elevations, where both
437 approaches predicted a series of drift and scour zones, although in sum, the MVR model
438 predicted greater SWE.
439



440 We used two different approaches to quantify the ‘time-stability’ of spatial patterns
441 across these glaciers. By the first metric, normalized range, we found that both glaciers
442 exhibited very similar patterns (Fig. 11), with either ~65 or 85 % (regression tree and
443 MVR, respectively) of the glacier area experiencing less than 25 % absolute normalized
444 variability (Fig. 12). The r^2 approach provides an alternative way of assessing the time
445 stability of SWE, essentially determining whether SWE at each location scales with the
446 glacier-wide value. By this metric, 80 % of the glacier area at Wolverine and 96 % of the
447 glacier area at Gulkana had a coefficient of determination greater than 0.8 (Fig. 12),
448 suggesting that most locations on the glacier have a consistent relationship with the mean
449 glacier-wide mass balance. By both metrics, the MVR output suggests greater temporal
450 stability (e.g., lower normalized range or higher r^2) compared to the regression tree.

451

452 **4.5. Winter mass balance**

453 In order to examine systematic variations between the approaches we outlined in Section
454 3 for calculating the glacier-wide winter balance, B_w , we first calculated a yearly mean
455 from the six approaches (including four based on the GPR observations: MVR,
456 regression tree, elevation gradient derived from centerline only observations, elevation
457 gradient derived from all point observations, and two based on the *in situ* stake network:
458 site-index and profile). In general, Gulkana exhibited greater agreement (4 % average
459 difference) among the approaches, with most approaches agreeing within 5 % of the six-
460 approach mean (Fig. 13; Table S2). Wolverine showed slightly less agreement (7 %
461 average difference), as the two terrain parameters statistical extrapolations (MVR and
462 regression tree) produced B_w estimates ~9 % above the mean, while the two stake derived
463 estimates were ~7 % less than the mean. On average across all five years at Wolverine,
464 the MVR approach was the most positive, while the glaciological site-index approach
465 was always the most negative (Fig. 13). At both glaciers, the estimates using elevation as
466 the only predictor yielded B_w estimates on average within 3 % of the six-method mean,
467 with the centerline only based estimate being slightly negatively biased, and the complete
468 observations being slightly positively biased.

469



470 To examine the systematic difference between the glaciological site-index method and
471 GPR-based MVR approach, we compared stake-derived b_w values from the three long-
472 term stakes to all GPR-based MVR b_w values within that index zone (Fig. 14). Both the
473 stakes and the GPR-derived b_w values have been normalized by the glacier-wide value to
474 make these results comparable across years and glaciers. It is apparent that Wolverine
475 experienced much greater spatial variability in accumulation, with larger interquartile
476 ranges and a large number of positive outliers in all index zones. Importantly, the stake
477 weight in the site-index solution is dependent on the hypsometry of the glacier, and for
478 both glaciers, the upper stake accounts for ~65% of the weighted average. In years that
479 the misfit between GPR B_w and site-index B_w was largest (2015 and 2016 at Gulkana,
480 2013 and 2017 at Wolverine), the stake-derived b_w at the upper stake was in the lower
481 quartile of all GPR-derived b_w values, explaining the significant difference in B_w
482 estimates in these years. Potential reasons for this discrepancy are discussed in Section
483 5.3.

484

485 *In situ* stake and pit observations traditionally serve as the primary tool for deriving
486 glaciological mass balances. However, in order for these observations to provide a
487 systematic and meaningful long-term record, they need to record interannual variability
488 in mass balance rather than interannual spatial variability in mass balance. To assess the
489 performance of the long-term stake sites, we examined the interannual variability metrics
490 for the stake locations. By both metrics (normalized absolute range and r^2), the middle
491 and upper elevation stakes at both glaciers appear to be in locations that achieve this
492 temporal stability, having exhibited ~10 % range and $r^2 > 0.95$ over the five-year interval.
493 The lower elevation stake was less temporally stable and exhibited opposing behavior at
494 each glacier. At Gulkana, this stake had a high r^2 (0.93) and moderate normalized
495 variability (26 %), which in part, reflects the lower total accumulation at this site and the
496 ability for a single uncharacteristic storm to alter this total amount significantly. In
497 contrast, Wolverine lowest site exhibited both low r^2 (< 0.01) and normalized range (2 %),
498 a somewhat unlikely combination. The statistical extrapolation approaches frequently
499 predicted zero or near-zero cumulative winter accumulation at this site (i.e., mid-winter



500 rain and/or ablation is common at this site), so although the normalized range was quite
501 low, predicted SWE values were uncorrelated with B_w over the study interval.

502

503 **Discussion**

504 **5.1. Interannual variability in spatial patterns**

505 Each glacier exhibited consistent normalized SWE spatial patterns across the five-year
506 study, reflecting the strong control of elevation and regular patterns in wind redistribution
507 in this complex topography (Fig. 11, S7, S8). This is particularly notable given the highly
508 variable magnitudes of accumulation over the five-year study and the contrasting climate
509 regions of these two glaciers (wet, warm maritime and cold, dry continental), with unique
510 storm paths, timing of annual accumulation, wind direction and wind direction
511 variability, and snow density. At both glaciers, the lowest interannual variability was
512 found away from locations with complex topography and elevated surface roughness,
513 such as crevassed zones, glacier margins, and areas near peaks and ridges.

514

515 In the most directly comparable study using repeat GPR surveys at Switzerland's
516 Findelgletscher, 86 % of the glacier area experienced less than 25 % range in relative
517 normalized accumulation over a three-year interval (Sold et al., 2016). As noted in
518 Section 3.4., we reported an absolute normalized range, whereas Sold et al. (2016)
519 reported a relative normalized range. Following their calculation, we found that 81 and
520 82 % of Wolverine and Gulkana's area experienced a relative normalized range less than
521 25 %. Collectively, our results add to the growing body of evidence (e.g., Deems et al.,
522 2008; Sturm and Wagner, 2010; Schirmer et al., 2011; Winstral and Marks, 2014)
523 suggesting 'time-stability' in the spatial distribution of snow in locations that span a
524 range of climate zones, topographic complexity, and relief. While the initial effort
525 required to constrain the spatial distribution over a given area can be significant, the
526 benefits of understanding the spatial distribution are substantial and long-lasting, and
527 have a wide range of applications.

528

529 **5.1.1 Elevation**



530 Elevation explained between 50 and 83 % of the observed SWE variability at Gulkana
531 and Wolverine, making it the most significant terrain parameter at both glaciers every
532 year (Fig. 4, 6). Exceptionally steep SWE gradients characterized both glaciers, annually
533 exceeding reported orographic precipitation gradients in other mountainous regions by a
534 factor of 2–3 (e.g., Anderson et al., 2014; Grünewald and Lehning, 2011). These steep
535 gradients are the result of physical processes beyond just orographic precipitation,
536 including storm systems that deliver snow at upper elevations and rain at lower elevations
537 (common at both Wolverine and Gulkana) and mid-winter ablation at lower elevations (at
538 Wolverine). These processes have been shown to steepen observed SWE gradients
539 relative to orographic precipitation gradients in a mid-latitude seasonal snow watershed
540 (Anderson et al., 2014). Unfortunately, given that we solely sampled snow distribution at
541 the end of the accumulation season, the relative magnitude of each of these secondary
542 processes is poorly constrained.

543
544 Wolverine and Gulkana glaciers exhibited opposing SWE gradients at their highest
545 elevations, with Wolverine showing a sharp non-linear increase in SWE, while Gulkana
546 showed a gradual decrease. This behavior was also noted at other maritime glaciers (Scott
547 and Valdez) in 2013 (McGrath et al., 2015), and perhaps reflects an abundance of split
548 precipitation phase storms in these warm coastal regions. The cause of the observed
549 reverse gradient at Gulkana may be the result of wind scouring at the highest and most
550 exposed sections of the glacier, or in part, a result of where we were able to safely sample
551 the glacier. For instance, in 2013, when we were able to access the highest basin on the
552 glacier, the SWE elevation gradient remained positive (Fig. 4).

553

554 **5.1.2. Wind redistribution**

555 Both statistical extrapolation approaches found terrain parameters Sb and curvature,
556 proxies for wind redistribution, to have the largest beta coefficients after elevation (Fig.
557 6, S9). The spatial pattern of SWE estimated by each model clearly reflects the dominant
558 influence of wind redistribution and elevation (Fig. 8), as areas of drift and scour are
559 apparent, especially at higher elevations. However, these terms do not fully capture the
560 redistribution process, as the model residuals (Fig. S1, S2) show sequential positive and



561 negative residuals associated with drift/scour zones. There are a number of reasons why
562 this might occur, including variable wind directions transporting snow (this is likely a
563 more significant issue at Gulkana, which experiences greater wind direction variability
564 (Fig. S6)), complex wind fields that are not well represented by a singular wind direction
565 (Dadic et al, 2010), changing surface topography (the glacier surface is dynamic over a
566 range of temporal scales, changing through both surface mass balance processes and ice
567 dynamics), and widely varying wind velocities. This is particularly relevant at Wolverine,
568 where wind speeds regularly gust over 30 m s^{-1} during winter storms, speeds that result in
569 variable length scales of redistribution that would not be captured by a fixed length scale
570 of redistribution. All of these factors influence the redistribution of snow and limit the
571 predictive ability of relatively simple proxies. Significant effort has gone into developing
572 physically-based snow-distribution models (e.g., Alpine3D and SnowModel), however,
573 high-resolution meteorological forcing data requirements generally limit the application
574 of these models in glacierized basins. Where such observations do exist, previous studies
575 have illuminated how the final distribution of snow is strongly correlated to the complex
576 wind field, including vertical (surface normal) winds (Dadic et al., 2010).

577

578 **5.1.3. Differences with non-glaciated terrain**

579 Although our GPR surveys did not include non-glaciated regions of these basins, a few
580 key differences are worth noting. First, the length scales of variability on and off the
581 glacier were distinctly different, with shorter scales and greater absolute variability
582 (snow-free to $>5 \text{ m}$ in less than 10 m distance) off-glacier (Fig. S10). This point has been
583 clearly shown using airborne LiDAR in a glaciated catchment in the Austrian Alps
584 (Helfricht et al., 2014). The reduced variability on the glacier is largely due to surface
585 mass balance and ice flow processes that act to smooth the surface, leading to a more
586 spatially consistent surface topography, and therefore a more spatially consistent SWE
587 pattern. In that way, measuring mean snowfall at a specific elevation and establishing the
588 elevation gradient in SWE on a glacier is often much less prone to terrain-induced
589 outliers (if obvious outlier locations, like icefalls, are avoided) than it is off-glacier.

590

591 **5.2. Spatial differences between statistical models**



592 The two statistical extrapolation approaches yielded comparable large-scale spatial
593 distributions and glacier-wide averages, although there were some notable spatial
594 differences (Fig. 10). The systematic positive bias of the MVR approach over the
595 regression tree at Wolverine was due to three sectors of the glacier with both complex
596 terrain (i.e., icefalls) and large data gaps (typically not safe to access on ground surveys).
597 The difference in predicted SWE in these locations is likely due to how the two statistical
598 extrapolation approaches handle unsampled terrain parameter space. The MVR
599 extrapolates based on global linear trends, while the regression tree assigns SWE from
600 terrain that most closely resembles the under sampled location. Anecdotally, it appears
601 that the MVR may overestimate SWE in some of these locations, which is most evident
602 in Wolverine's lower icefall, where bare ice is frequently exposed at the end of the
603 accumulation season (Fig. S11) in locations where the MVR predicted substantial SWE.
604 Likewise, the regression tree models could be underestimating SWE in these regions, but
605 in the absence of direct observations the errors are inherently unknown. The regression
606 tree model captures more short length scale variability while the MVR model clarifies the
607 larger trends. Consequently, smaller drifts and scours are captured well by the regression
608 tree model in areas where the terrain parameter space is well surveyed, but the results
609 become progressively less plausible as the terrain becomes more different from the
610 sampled terrain parameter space. In contrast, the MVR model appears to give more
611 plausible results at larger spatial scales. This suggests that there is some theoretical
612 threshold where the regression tree is more appropriate if the terrain parameter space is
613 sampled sufficiently, but that for many glacier surveys the MVR model would be more
614 appropriate.

615

616 **5.3. Winter mass balance comparisons**

617 On average, all methods for estimating B_w were within $\pm 11\%$ of the six-method mean,
618 (Fig. 13). The agreement (as measured by the average percent difference from the mean)
619 between estimates was slightly better at Gulkana than Wolverine, likely reflecting the
620 overall lower spatial variability at Gulkana and the greater percentage of the glacier area
621 where b_w correlates well with the glacier-wide average (Fig. 11 e, f). At both glaciers, B_w



622 solutions based solely on elevation showed excellent agreement to the six-method mean,
623 suggesting that this simple approach is a viable means for measuring B_w on these glaciers.
624 The biggest differences occurred between the GPR-forced MVR model and the
625 glaciological site-index method, which we've shown is attributed to the upper stake (with
626 the greatest weight) underestimating the median SWE for that index zone (Fig. 14). The
627 upper stake location was established in 1966 at an elevation below the median elevation
628 of that index zone, which given the strong elevation control on SWE, is a likely reason
629 for the observed difference. At Gulkana, the relationship between the upper index site
630 and the GPR-forced MVR model is more variable in large part due to observed
631 differences in the accumulation between the main branch (containing the index site) and
632 the west branch of the glacier. In the context of the MVR model, this manifests as a
633 change in sign in the eastness coefficient (which separates the branches in parameter
634 space; Fig. S4). Notably, in the two years where the site-index estimate was most
635 negatively biased at Gulkana (2015 and 2016), the glaciological profile method, relying
636 on the more extensive stake network (which includes stakes in the west branch of the
637 glacier), yielded B_w estimates within a few percent of the GPR-derived MVR estimate.
638
639 These B_w results have important implications for the glaciological mass balance time-
640 series, which is calibrated with geodetic observations (O'Neel et al., 2014). At
641 Wolverine, stake solutions are positively biased compared to the geodetic mass balance
642 solution, requiring a negative calibration ($-0.43 \text{ m w.e. a}^{-1}$; O'Neel et al., 2014). If the
643 GPR-derived solutions are assumed to be the most accurate estimate of B_w , this misfit
644 would be further increased by $-0.4 \text{ m w.e. a}^{-1}$ (the mean difference between MVR and
645 site-index B_w estimates), suggesting that the stakes are underestimating ablation (B_s) by
646 $\sim 1 \text{ m w.e. a}^{-1}$. This suggests some sectors of the glacier experience very high ablation
647 rates that are not captured by the stake network (e.g., crevassed zones through enhanced
648 shortwave solar radiation gain (e.g., Pfeffer and Bretherton, 1987; Cathles et al., 2011;
649 Colgan et al., 2016), and/or increased turbulent heat fluxes due to enhanced surface
650 roughness), and/or ice margins (through enhanced longwave radiation from nearby snow-
651 free land cover)). However, these results are not universal, as the assimilation of
652 distributed GPR observations at Findelgletcher significantly improved the comparison



653 between geodetic and modeled mass balance estimates (Sold et al., 2016), suggesting
654 multiple drivers of glaciologic-geodetic mismatch for long-term mass balance programs.
655

656 **5.3.1. Implications for stake placement**

657 Understanding the spatiotemporal distribution of SWE is useful for informing stake
658 placements and also for quantifying the uncertainty that interannual spatial variations in
659 SWE introduce to historic estimates of glacier-wide mass balance, particularly when
660 long-term mass balance programs rely on limited numbers of point observations (e.g.,
661 USGS and National Park Service glacier monitoring programs; O’Neel et al., 2014;
662 Burrows, 2014). Our winter balance results illustrate that stakes placed at the same
663 elevation are not directly comparable, and hence are not necessarily interchangeable in
664 the context of a multi-year mass balance record. Most locations on the glacier exhibit bias
665 from the average mass balance at that elevation and our results suggest interannual
666 consistency in this bias over sub-decadal time scales. As a result, constructing a balance
667 profile using a small number of inconsistently located stakes is likely to introduce large
668 relative errors from one year to the next.

669
670 Considering this finding, the placement of stakes to measure snow accumulation is
671 dependent on whether a single glacier-wide winter mass balance value (B_w) or a spatially
672 distributed SWE field is desired as a final product. For the former, a small number of
673 stakes can be distributed over the glacier hypsometry in areas where interannual
674 variability is low. Alternatively, if a distributed field is desired, a large number of stakes
675 can be widely distributed across the glacier, including areas where the interannual
676 variability is higher. In both cases it is important to have consistent locations from year to
677 year, although as the number of stakes increases significantly, this becomes less critical.

678
679 We assess the uncertainty that interannual variability in the spatial distribution of SWE
680 introduces to the historic index-method (March and Trabant, 1996) mass balance
681 solutions by first calculating the uncertainty, σ , contributed by each stake as:

$$682 \sigma_{stake} = \sigma_{model\ residuals} + (1 - r^2) \cdot u, \quad (3)$$



683 where $\sigma_{model\ residuals}$ is the standard deviation of MVR model residuals over all five
684 years within ± 30 meters of the index site, u is the mean b_w within ± 30 meters of the
685 index site, and r^2 is the coefficient of determination between b_w and B_w over the five-year
686 period (Fig. 11). The first term on the right hand side of Eq. 3 accounts for both the
687 spatial and temporal variability in the observed b_w as compared to the model, and the
688 second term accounts for the variability of the model as compared to B_w . The glacier-
689 wide uncertainty from interannual variability is then:

$$690 \text{ Glacier } \sigma = \sqrt{\sum_{all\ stakes} (\sigma_{stake} \cdot w_{stake})^2}, \quad (4)$$

691 where w_{stake} is the weight function from the site-index method (which depends on stake
692 location and glacier hypsometry). By this assessment, interannual variability in the spatial
693 distribution of SWE at stake locations introduced minor uncertainty, on the order of 0.11
694 m w.e. at both glaciers (4 % and 10 % of B_w at Wolverine and Gulkana, respectively).
695 This suggests that the original stake network design at the benchmark glaciers does
696 remarkably well at capturing the interannual variability in glacier-wide winter balance.
697 The greatest interannual variability at each glacier is found at the lowest stake sites, but
698 because b_w and the stake weights are both quite low at these sites, they contribute only
699 slightly to the overall uncertainty. Instead, the middle and upper elevation stakes
700 contribute the greatest amount to the glacier-wide uncertainty.

701

702 6. Conclusions

703 We collected spatially extensive GPR observations at two glaciers in Alaska for five
704 consecutive winters to quantify the spatiotemporal distribution of SWE. We found good
705 agreement of glacier-average winter balances, B_w , among the four different approaches
706 used to extrapolate GPR point measurements of SWE across the glacier hypsometry.
707 Extrapolations relying only on elevation (i.e., a simple balance profile) produced B_w
708 estimates similar to the more complicated statistical models, suggesting that this is an
709 appropriate method for quantifying glacier-wide winter balances at these glaciers. The
710 more complicated approaches, which allow SWE to vary across a range of terrain-
711 parameters based on DEMs, show a high degree of temporal stability in the pattern of
712 accumulation at both glaciers, as ~ 85 % of the area on both glaciers experienced less than
713 25 % normalized absolute variability over the five-year interval. Elevation and the



714 parameters related to wind redistribution had the most explanatory power, and were
715 temporally consistent at each site. The choice between MVR and regression tree models
716 should depend on both the range in terrain-parameter space that exists on the glacier,
717 along with how well that space is surveyed.

718

719 In total, six different methods (four based on GPR measurements and two based on stake
720 measurements) for estimating the glacier-wide average agreed within ± 11 %. The site-
721 index glaciological B_w estimates were negatively biased compared to all other estimates,
722 particularly when the upper-elevation stake significantly underestimated SWE in that
723 index zone. In contrast, the profile glaciological approach, using a more extensive stake
724 network, showed better agreement with the other approaches, highlighting the benefits of
725 using a more extensive stake network.

726

727 We found the spatial patterns of snow accumulation to be temporally stable on these
728 glaciers, which is consistent with a growing body of literature documenting similar
729 consistency in a wide variety of environments. The long-term stake locations experienced
730 low interannual variability in normalized SWE, meaning that stake measurements
731 tracked the interannual variability in SWE, rather than interannual variability in spatial
732 patterns. The uncertainty associated with interannual spatial variability is only 4–10 % of
733 the glacier-wide B_w at each glacier. Thus, our findings support the concept that sparse
734 stake networks can be effectively used to measure interannual variability in winter
735 balance on glaciers.

736

737 *Data Availability.* The GPR and associated observational data used in this study can be
738 accessed on the USGS Glaciers and Climate Project website
739 (<https://doi.org/10.5066/F7M043G7>). The Benchmark Glacier mass balance input and
740 output can be accessed at: <https://doi.org/10.5066/F7HD7SRF> (O’Neel et al., 2018). The
741 Gulkana DEM is available from the ArcticDEM project website
742 (<https://www.pgc.umn.edu/data/arcticdem/>) and the Wolverine DEM will be available at
743 arctic.io (link pending).

744



745 *Author Contributions.* SO, DM, LS, and HPM designed the study. DM performed the
746 analyses and wrote the manuscript. LS contributed to the design and implementation of
747 the analyses, and CM, SC, and EHB contributed specific components of the analyses. All
748 authors provided feedback and edited the manuscript.

749

750 *Competing Interests.* The authors declare that they have no conflict of interest.

751

752 *Acknowledgments.* This work was funded by the U.S. Geological Survey Land Change
753 Science Program, USGS Alaska Climate Adaptation Science Center, and DOI/USGS
754 award G17AC00438 to DM. Any use of trade, firm, or product names is for descriptive
755 purposes only and does not imply endorsement by the U.S. Government. We
756 acknowledge the Polar Geospatial Center (NSF-OPP awards 1043681, 1559691, and
757 1542736) for the Gulkana DEM.

758

759 **References**

760

761 Akaike, H.: A new look at the statistical model identification, *IEEE Trans. Autom.*
762 *Control*, AC-19(6), 1974.

763

764 Anderson, B. T., McNamara, J. P., Marshal, H. P., and Flores, A. N.: Insights into the
765 physical processes controlling correlations between snow distribution and terrain
766 properties, *Water Res. Res.*, 50(6), 4545–4563, doi:10.1002/2013WR013714, 2014.

767

768 Bair, E. H., Calfa, A. A., Rittger, K., and Dozier, J.: Using machine learning for real-time
769 estimates of snow water equivalent in the watersheds of Afghanistan, *The Cryosphere*,
770 12, 1579–1594, doi:10.5194/tc-12-1579-2018, 2018.

771

772 Balk, B. and Elder, K.: Combining binary regression tree and geostatistical methods to
773 estimate snow distribution in a mountain watershed, *Water Res. Res.*, 36(1), 13–26, 2000.

774

775 Burrows, R.: Annual report on vital signs monitoring of glaciers in the Central Alaska
776 Network 2011–2013, Natural Resource Technical Report NPS/CAKN/NRTR—2014/905,
777 National Park Service, Fort Collins, Colorado, 2014.



- 778
779 Breiman, L.: Bagging predictors, *Mach. Learn.*, 24, 123–140,
780 <https://doi.org/10.1023/A:1018054314350>, 1996.
781
782 Breiman, L.: Random forests, *Mach. Learn.*, 45, 5–32,
783 <https://doi.org/10.1023/A:1010933404324>, 2001.
784
785 Breiman, L., Friedman, J. H., Olshen, R. A., and Stone, C. J.: Classification and
786 Regression Trees, Chapman and Hall, New York, 368 pp., 1984.
787
788 Cathles, L. C., Abbot, S. D., Bassis, J. N., and MacAyeal, D.R.: Modeling surface-
789 roughness/solar-ablation feedback: application to small-scale surface channels and
790 crevasses of the Greenland ice sheet, *Ann. Glaciol.*, 52(59), 99–108, 2011.
791
792 Cogley, J. G., Hock, R., Rasmussen, L. A., Arendt, A. A., Bauder, A., Braithwaite, R. J.,
793 Jansson, P., Kaser, G., Möller, M., Nicholson, L. and Zemp, M.: Glossary of Glacier
794 Mass Balance and Related Terms, IHP-VII Technical Documents in Hydrology No. 86,
795 IACS Contribution No. 2, UNESCO-IHP, Paris, 2011.
796
797 Colgan, W., Rajaram, H., Abdalati, W., McCutchan, C., Mottram, R., Moussavi, M. S.,
798 and Grigsby, S.: Glacier crevasses: Observations, models, and mass balance implications,
799 *Rev. Geophys.*, 54, doi:10.1002/2015RG000504, 2016.
800
801 Dadic, R., Mott, R., Lehning, M., and Burlando, P.: Wind influence on snow depth
802 distribution and accumulation over glaciers, *J. Geophys. Res.*, 115, F01012,
803 doi:10.1029/2009JF001261, 2010.
804
805 Deems, J. S., Fassnacht, S. R., and Elder, K. J.: Interannual consistency in fractal snow
806 depth patterns at two Colorado mountain sites, *J. Hydromet.*, 9, 977–988,
807 doi:10.1175/2008JHM901.1, 2008.
808



- 809 Elder, K., Michaelsen, J., and Dozier, J.: Small basin modeling of snow water
810 equivalence using binary regression tree methods, *IAHS Publ.* 228, 129–139, 1995.
811
- 812 Erickson, T. A., Williams, M.W., and Winstral, A.: Persistence of topographic controls
813 on the spatial distribution of snow in rugged mountain terrain, Colorado, United States,
814 *Water Res. Res.*, 41, W04014, doi:10.129/2003WR002973, 2005.
- 815 Fitzpatrick, N., Radić, V., and Menounos, B.: Surface energy balance closure and
816 turbulent flux parameterization on a mid-latitude mountain glacier, Purcell Mountains,
817 Canada, *Front. Earth Sci.*, 5(67), doi:10.3389/feart.2017.00067, 2017.
- 818 Grünewald, T., and Lehning, M.: Altitudinal dependency of snow amounts in two alpine
819 catchments: Can catchment-wide snow amounts be estimated via single snow or
820 precipitation stations?, *Ann. Glaciol.*, 52(58), 153–158, 2011.
- 821 Helfricht, K., Schöber, J., Schneider, K., Sailer, R., and Kuhn, M.: Interannual
822 persistence of the seasonal snow cover in a glacierized catchment, *J. Glaciol.*, 60(223),
823 doi:10.3189/2014JoG13J197, 2014.
824
- 825 Hock, R.: Glacier melt: a review of processes and their modeling, *Prog. Phys. Geog.*, 29,
826 362–391, doi:10.1191/0309133305pp453ra, 2005.
827
- 828 Hock, R., Hutchings, J. K., and Lehning, M.: Grand challenges in cryospheric sciences:
829 toward better predictability of glaciers, snow and sea ice, *Front. Earth Sci.*, 5(64),
830 doi:10.3389/feart.2017.00064, 2017.
831
- 832 Hodgkins, R., Cooper, R., Wadham, J., and Tranter, M.: Interannual variability in the
833 spatial distribution of winter accumulation at a high-Arctic glacier (Finsterwalderbreen,
834 Svalbard), and its relationship with topography, *Ann. Glaciol.*, 42, 243–248, 2005.
835
- 836 Huss, M. and Hock, R.: A new model for global glacier change and sea-level rise, *Front.*
837 *Earth Sci.*, 3, doi:10.3389/feart.2015.00054, 2015.



- 838 Kaser, G., Großhauser, M., and Marzeion, B.: Contribution potential of glaciers to water
839 availability in different climate regimes, *Proc. Natl. Acad. Sci.*, 107, 20,223–20,227,
840 doi:10.1073/pnas.1008162107, 2010.
- 841
- 842 Klos, P. Z., Link, T. E., and Abatzoglou, J. T.: Extent of the rain-snow transition zone in
843 the western U.S. under historic and projected climate, *Geophys. Res. Lett.*, 41, 4560–
844 4568, doi: 10.1002/2014GL060500, 2014.
- 845
- 846 Knowles, N., Dettinger, M. D., and Cayan, D. R.: Trends in snowfall versus rainfall in
847 the Western United States, *J. Climate*, 19, 4545–4559, 2006.
- 848
- 849 Kovacs, A., Gow, A. J., and Morey, R. M.: The in-situ dielectric constant of polar firn
850 revisited, *Cold Reg. Sci. Tech.*, 23, 245–256, 1995.
- 851
- 852 Kuhn, M.: The mass balance of very small glaciers, *Z. Gletscherkd. Glazialgeol.*, 31(1–
853 2), 171–179, 1995.
- 854
- 855 Lehning, M., Grünewald, T., and Schirmer, M.: Mountain snow distribution governed by
856 altitudinal gradient and terrain roughness, *Geophys. Res. Lett.*, 38, L19504,
857 doi:10.1029/2011GL048927, 2011.
- 858
- 859 Li, L. and Pomeroy, J. W.: Estimates of threshold wind speeds for snow transport using
860 meteorological data, *J. Applied Met.*, 36, 205–213, 1997.
- 861
- 862 Liston, G. E., and Elder, K.: A distributed snow-evolution modeling system
863 (SnowModel), *J. Hydromet.*, 7, 1259–1276, 2006.
- 864
- 865 Littel, J. S., McAfee, S. A., and Hayward, G. D.: Alaska snowpack response to climate
866 change: statewide snowfall equivalent and snowpack water scenarios, *Water*, 10 (5), doi:
867 10.3390/w10050668, 2018.
- 868



- 869 Marks, D., Domingo, J., Susong, D., Link, T., and Garen, D.: A spatially distributed
870 energy balance snowmelt model for application in mountain basins, *Hydrol. Processes*,
871 13, 1935–1959, 1999.
- 872
- 873 Machguth, H., Eisen, O., Paul, F., and Hoelzle, M.: Strong spatial variability of snow
874 accumulation observed with helicopter-borne GPR on two adjacent Alpine glaciers,
875 *Geophys. Res. Lett.*, 33, L13503, doi:10.1029/2006GL026576, 2006.
- 876
- 877 March, R. S., and Trabant, D. C.: Mass balance, meteorological, ice motion, surface
878 altitude, and runoff data at Gulkana Glacier, Alaska, 1992 balance year, *Water-Resources*
879 *Investigations Report*, 95-4277, 1996.
- 880
- 881 McAfee, S., Walsh, J., and Rupp, T. S.: Statistically downscaled projections of snow/rain
882 partitioning for Alaska, *Hydrol. Process.*, 28(12), 3930–3946, doi:10.1002/hyp.9934,
883 2013.
- 884
- 885 McGrath, D., Sass, L., O’Neel, S., Arendt, A., Wolken, G., Gusmeroli, A., Kienholz, C.,
886 and McNeil, C.: End-of-winter snow depth variability on glaciers in Alaska, *J. Geophys.*
887 *Res. Earth Surf.*, 120, 1530–1550, doi:10.1002/2015JF003539, 2015.
- 888
- 889 McGrath, D., Sass, L., O’Neel, S., Arendt, A. and Kienholz, C.: Hypsometric control on
890 glacier mass balance sensitivity in Alaska and northwest Canada, *Earth’s Future*, 5, 324–
891 336, doi:10.1002/2016EF000479, 2017.
- 892
- 893 Meromy, L., Molotch, N. P., Link, T. E., Fassnacht, S. R., and Rice, R.: Subgrid
894 variability of snow water equivalent at operational snow stations in the western USA,
895 *Hydro. Proc.*, 27, 2383-2400, doi:10.1002/hyp.9355, 2013.
- 896
- 897 Molotch, N. P., Colee, M. T., Bales, R. C. and Dozier, J.: Estimating the spatial
898 distribution of snow water equivalent in an alpine basin using binary regression tree



- 899 models: the impact of digital elevation data and independent variable selection, *Hydrol.*
900 *Proc.*, 19, 1459–14-79, doi:10.1002/hyp.5586, 2005.
- 901
- 902 Nolan, M., Larsen, C., and Sturm, M.: Mapping snow depth from manned aircraft on
903 landscape scales at centimeter resolution using structure-from-motion photogrammetry,
904 *The Cryosphere*, 9, 1445-1463, doi:10.5194/tc-9-1445-2015, 2015.
- 905
- 906 Noh, M. J. and Howat, I. M.: Automated stereo-photogrammetric DEM generation at
907 high latitudes: Surface Extraction with TIN-based Search-space Minimization (SETSM)
908 validation and demonstration over glaciated regions, *GIScience & Remote*
909 *Sensing*, 52(2), 198-217, doi:10.1080/15481603.2015.1008621, 2015.
- 910
- 911 O’Neel, S., Hood, E., Arendt, A., and Sass, L.: Assessing streamflow sensitivity to
912 variations in glacier mass balance, *Climatic Change*, 123(2), 329–341,
913 doi:10.1007/s10584-013-1042-7, 2014.
- 914
- 915 O’Neel, S., Fagre, D. B., Baker, E. H., Sass, L. C., McNeil, C. J., Peitzsch, E. H.,
916 McGrath, D. and Florentine, C. E.: Glacier-Wide Mass Balance and Input Data: USGS
917 Benchmark Glaciers, 1966-2016 (ver. 2.1, May 2018), U.S. Geological Survey data
918 release, <https://doi.org/10.5066/F7HD7SRE>, 2018.
- 919
- 920 Painter, T., Berisford, D., Boardman, J., Bormann, K., Deems, J., Gehrke, F., Hedrick,
921 A., Joyce, M., Laidlaw, R., Marks, D., Mattmann, C., Mcgurk, B., Ramirez, P.,
922 Richardson, M., Skiles, S.M., Seidel, F., and Winstral, A.: The Airborne Snow
923 Observatory: fusion of scanning lidar, imaging spectrometer, and physically-based
924 modeling for mapping snow water equivalent and snow albedo, *Remote Sens. Environ.*,
925 184, 139–152, doi:10.1016/j.rse.2016.06.018, 2016.
- 926
- 927 Pérez-Ruiz, M., Carballido, J., and Agüera, J.: Assessing GNSS correction signals for
928 assisted guidance systems in agricultural vehicles, *Precision Agric.*, 12, 639–652,
929 doi:10.1007/s11119-010-9211-4, 2011.



930

931 Pfeffer, W. T., and Bretherton, C.: The effect of crevasses on the solar heating of a
932 glacier surface, *IAHS Publ.*, 170, 191–205, 1987.

933

934 Pfeffer, W. T., et al.: The Randolph Glacier Inventory: A globally complete inventory of
935 glaciers, *J. Glaciol.*, 60(221), 537–552, doi:10.3189/2014JoG13J176, 2014.

936

937 Schirmer, M., Wirz, V., Clifton, A., and Lehning, M.: Persistence in intra-annual snow
938 depth distribution: 1. Measurements and topographic control, *Water Resour. Res.*, 47,
939 W09516, doi:10.1029/2010WR009426, 2011.

940

941 Sold, L., Huss, M., Hoelzle, M., Anderegg, H., Joerg, P., and Zemp, M.:
942 Methodological approaches to infer end-of-winter snow distribution on alpine glaciers, *J.*
943 *Glaciol.*, 59(218), 1047–1059, doi:10.3189/2013JoG13J015, 2013.

944

945 Sold, L., Huss, M., Machguth, H., Joerg, P. C., Vieli, G. L., Linsbauer, A., Salzmann, N.,
946 Zemp, M. and Hoelzle, M.: Mass balance re-analysis of Findelengletscher, Switzerland;
947 Benefits of extensive snow accumulation measurements, *Front. Earth Sci.*, 4(18),
948 doi:10.3389/feart.2016.00018, 2016.

949

950 Sturm, M. and Wagner, A. M.: Using repeated patterns in snow distribution modeling:
951 An Arctic example, *Water Res. Res.*, 46 (12), doi:10.1029.2010WR009434, 2010.

952

953 Van Beusekom, A. E., O’Neel, S., March, R. S., Sass, L., and Cox, L. H.: Re-analysis of
954 Alaskan Benchmark Glacier mass balance data using the index method, U.S. Geological
955 Survey Scientific Investigations Report 2010–5247, 16 p., 2010.

956 Winstral, A., Elder, K., and Davis, R. E.: Spatial snow modeling of wind-redistributed
957 snow using terrain-based parameters, *J. Hydrometeo.*, 3, 524–538, 2002.

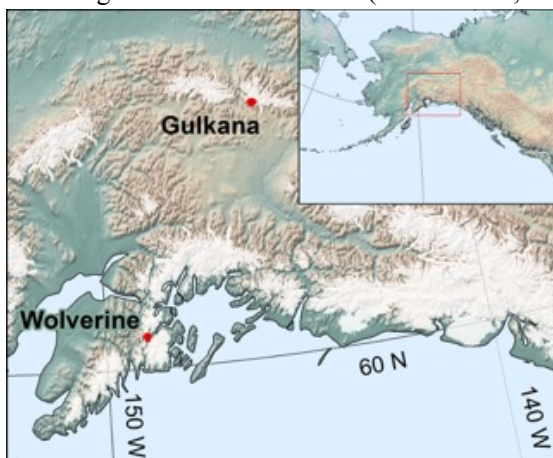
958



- 959 Winstral, A., Marks, D. and Gurney, R.: Simulating wind-affected snow accumulations at
960 catchment to basin scales, *Adv. Water Res.*, 55, 64–79,
961 doi:10.1016/j.advwatres.2012.08.011, 2013.
- 962
- 963 Winstral, A. and Marks, D.: Long-term snow distribution observations in a mountain
964 catchment: Assessing variability, time stability, and the representativeness of an index
965 site, *Water Res. Res.*, 50, 293–305, doi:1002/2012WR013038, 2014.
- 966
- 967 Woo, M.-K., and Marsh, P.: Analysis of error in the determination of snow storage for
968 small high Arctic basins, *J. Appl. Meteorol.*, 17, 1537–1541, 1978.
- 969
- 970 Yelf, R. and Yelf, D.: Where is true time zero?, *Electro. Phenom.*, 7(1), 158–163, 2006.
- 971
972
973
974
975
976
977
978
979
980
981
982
983
984
985
986
987
988
989
990
991
992
993
994

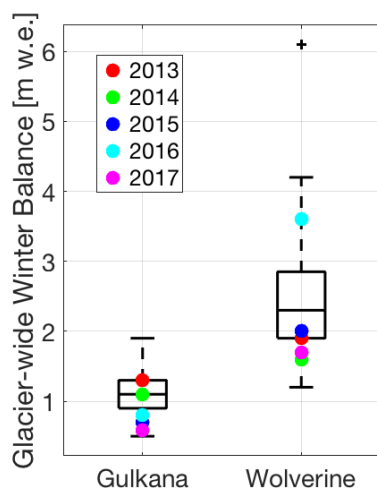


995 Figure 1. Map of southern Alaska with study glaciers marked by red outline. All glaciers
996 in the region are shown in white (Pfeffer et al., 2014).



997
998
999
1000
1001

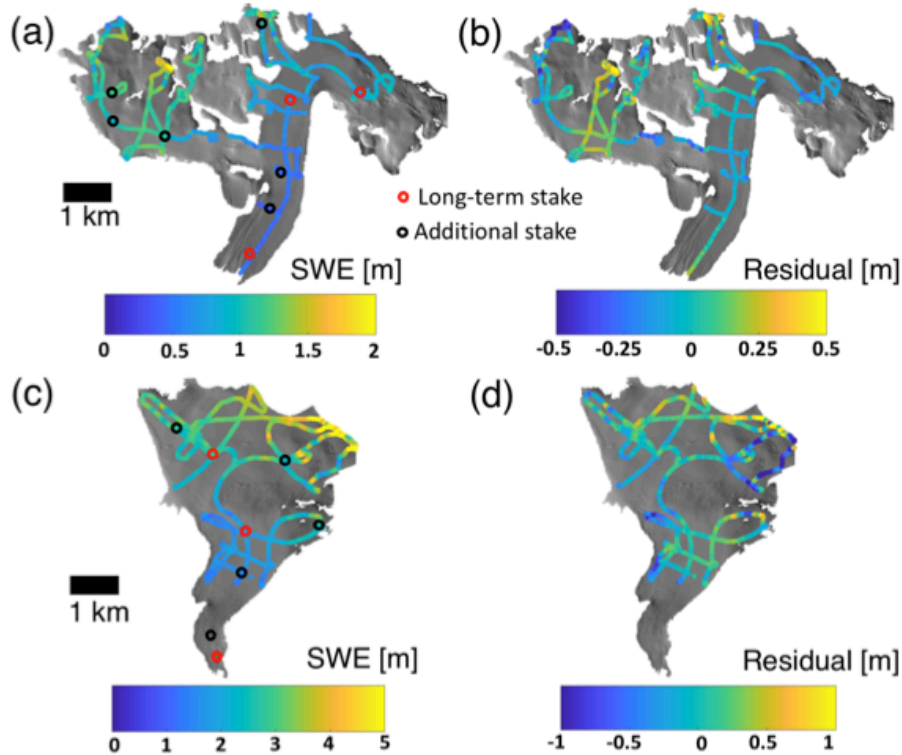
1002 Figure 2. Boxplots of glacier-wide winter balance for Gulkana and Wolverine glaciers
1003 between 1966 and 2017. Years corresponding to GPR surveys are shown with colored
1004 markers. These values have not been adjusted by the geodetic calibration (see O’Neel et
1005 al., 2014).



1006
1007
1008
1009

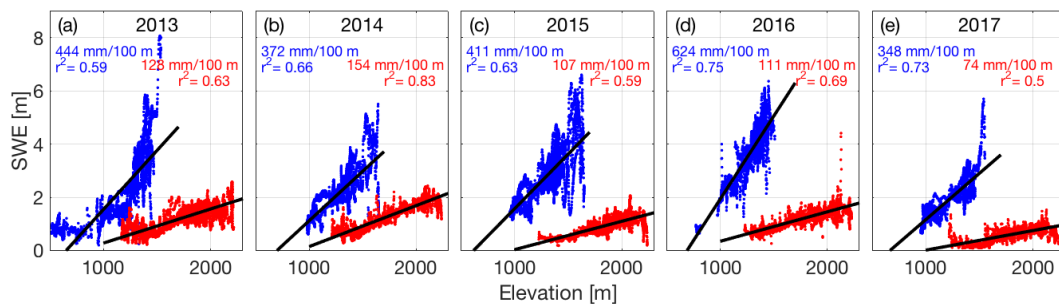


1010 Figure 3. GPR surveys from 2015 at Gulkana (a) and Wolverine (c) glaciers and MVR
 1011 model residuals (b, d).



1012
 1013
 1014

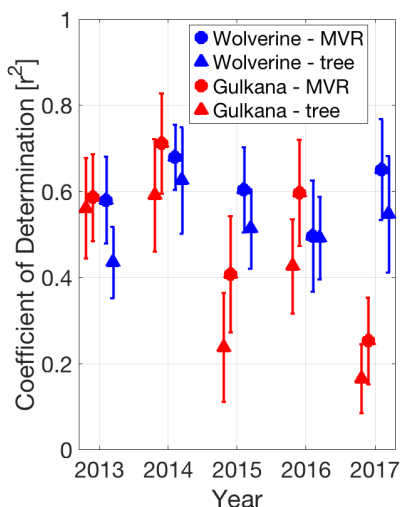
1015 Figure 4. SWE from GPR surveys as a function of elevation, along with least squares
 1016 regression slope and coefficient of determination for each year of the study period.
 1017 Wolverine is plotted in blue, Gulkana in red.



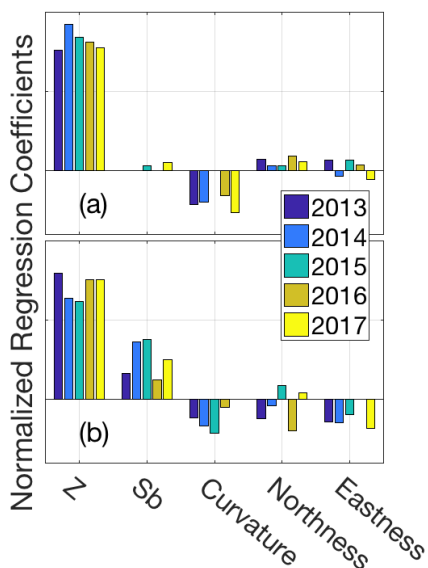
1018
 1019



1020 Figure 5. Median and standard deviation (error bars) of coefficient of determination
 1021 (from 100 model runs) for both extrapolation approaches (circles are MVR, triangles are
 1022 regression tree) developed on training datasets and applied to test datasets. Symbols and
 1023 error bars are offset from year for clarity.



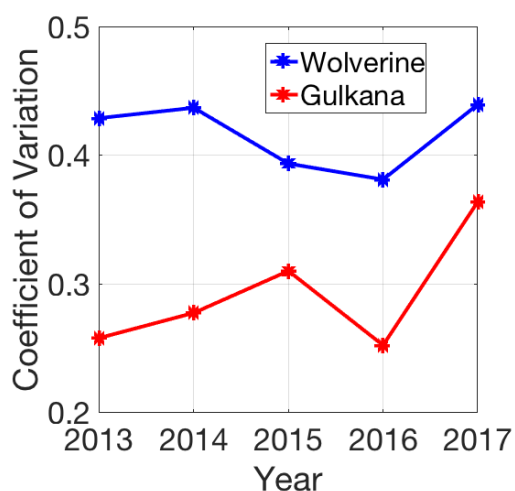
1024 Figure 6. Terrain parameter beta coefficients for (a) Gulkana and (b) Wolverine for
 1025 multivariable linear regression for each year of the study interval.
 1026



1027
 1028
 1029

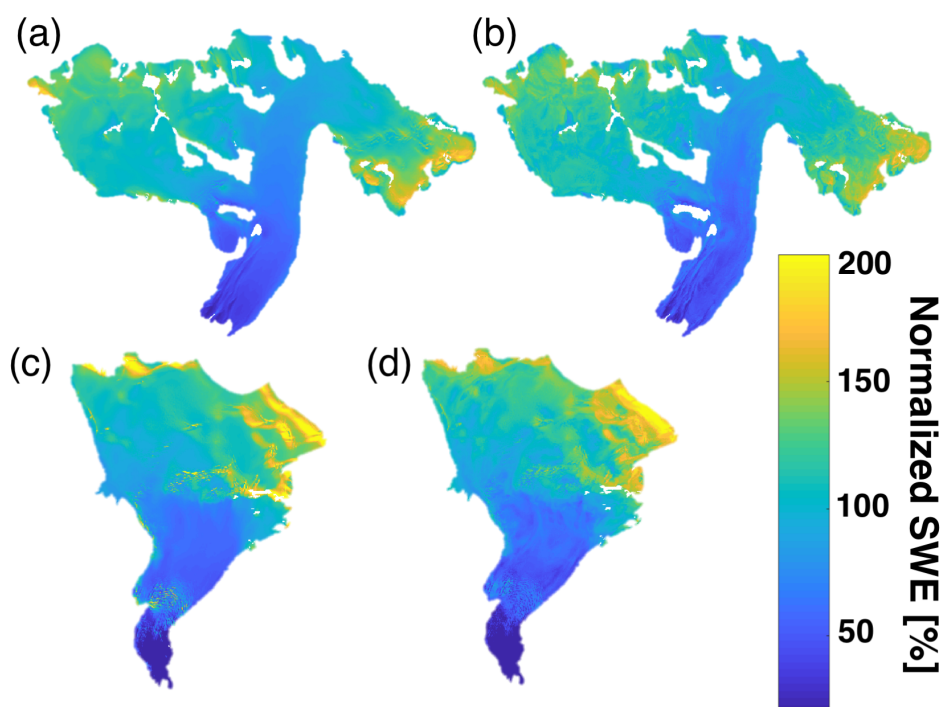


1030 Figure 7. Spatial variability in snow accumulation across the glacier quantified by the
1031 coefficient of variation (standard deviation/mean) for each glacier across the five-year
1032 interval based on MVR model output.
1033



1034
1035

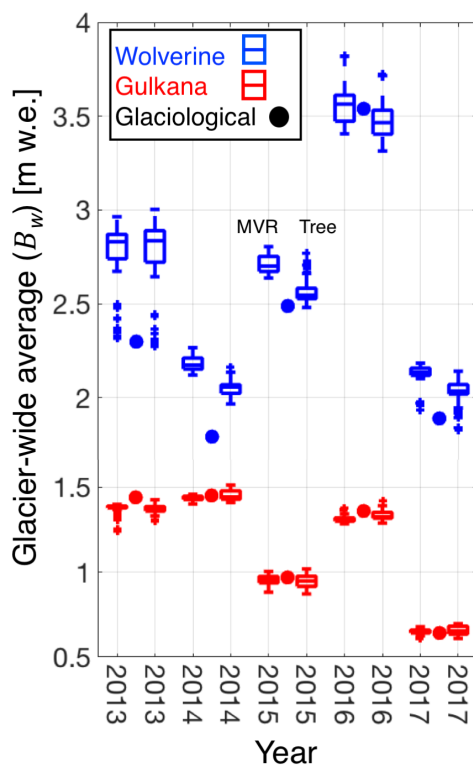
1036 Figure 8. Five-year mean of normalized distributed SWE for Gulkana (a,b) and
1037 Wolverine (c,d) for multivariable regression (a,c) and regression tree (b,d).



1038



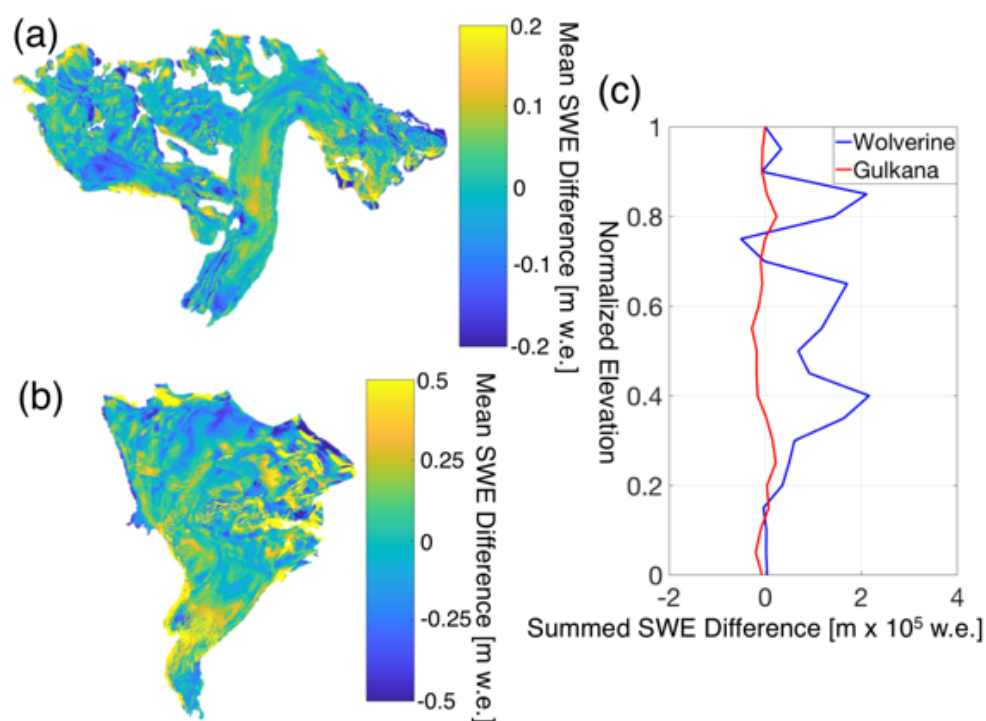
1039 Figure 9. Comparing statistical models for GPR-derived glacier-wide winter balances for
1040 both Wolverine (blue) and Gulkana (red) glaciers. For each year and each glacier, two
1041 boxplots are shown. The first shows multivariable regression model (MVR) output and
1042 the second shows regression tree output (tree). The B_w estimate from the glaciological
1043 profile method is shown for each year and glacier as the filled circle.
1044



1045
1046
1047
1048
1049
1050
1051
1052
1053
1054
1055



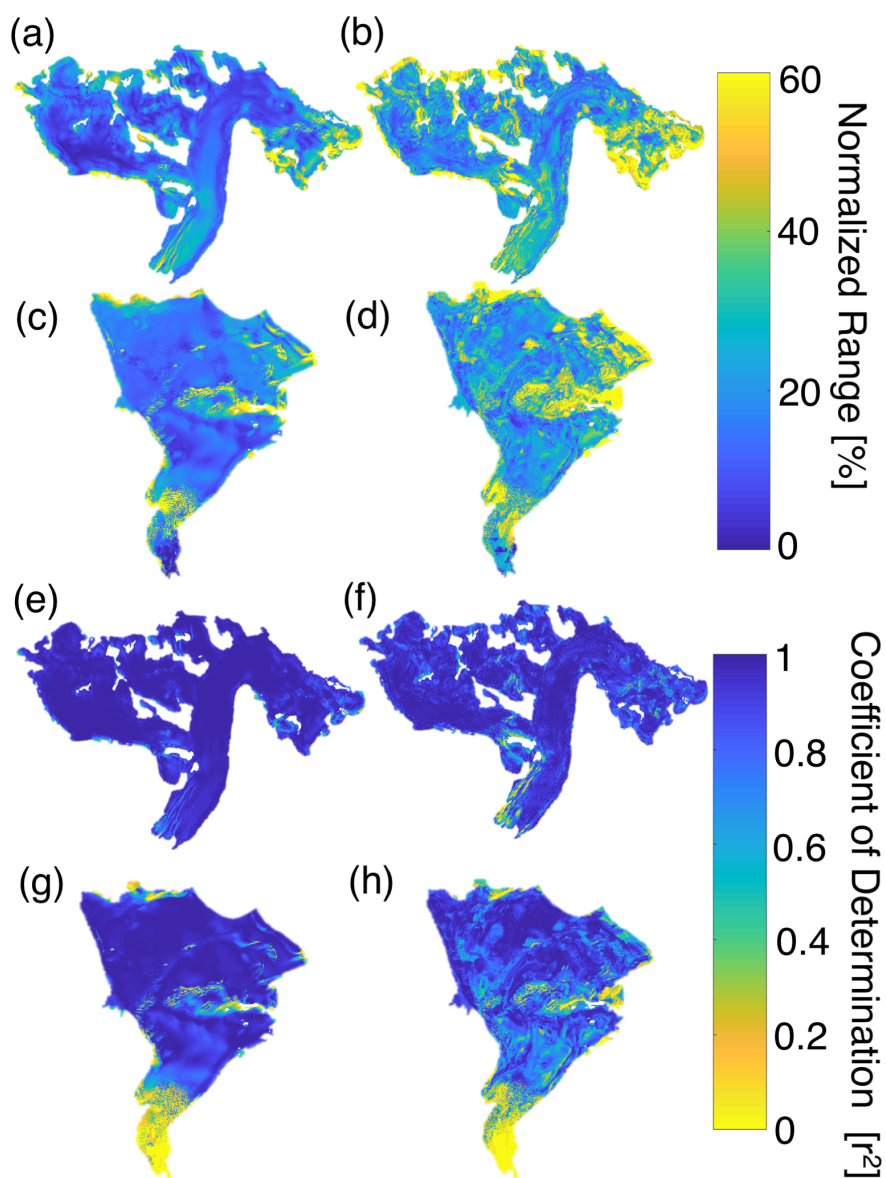
1056 Figure 10. SWE differences between statistical models for Gulkana (a) and Wolverine
1057 (b) calculated by differencing the regression tree five-year mean SWE from the
1058 multivariable regression (MVR) five-year mean SWE. Yellow colors indicate regions
1059 where MVR yields more SWE than decision tree and blue colors indicate the opposite.
1060 Note different magnitude colorbar scales. c) Summed SWE difference between methods
1061 in bins of 0.05 normalized elevation values.



1062
1063
1064
1065
1066
1067
1068
1069
1070
1071
1072
1073
1074
1075



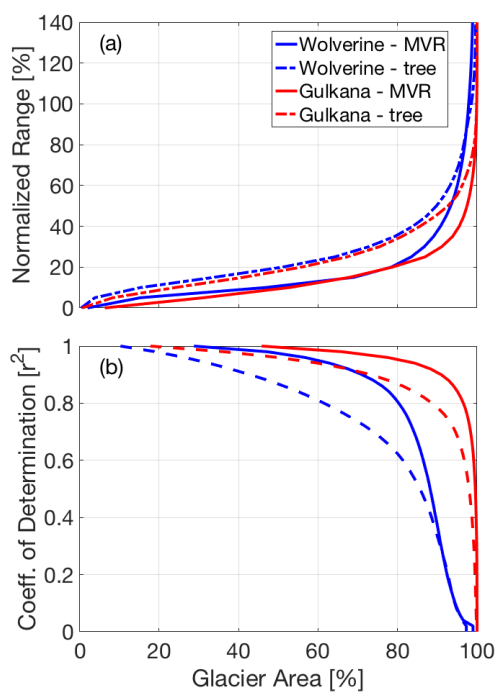
1076 Figure 11. Interannual variability of the SWE accumulation field from 2013-2017,
1077 quantified via normalized range (a-d) and r^2 (e-h) approach for median distributed fields
1078 from the multivariable regression (left column) and regression tree (right column)
1079 statistical models.
1080



1081



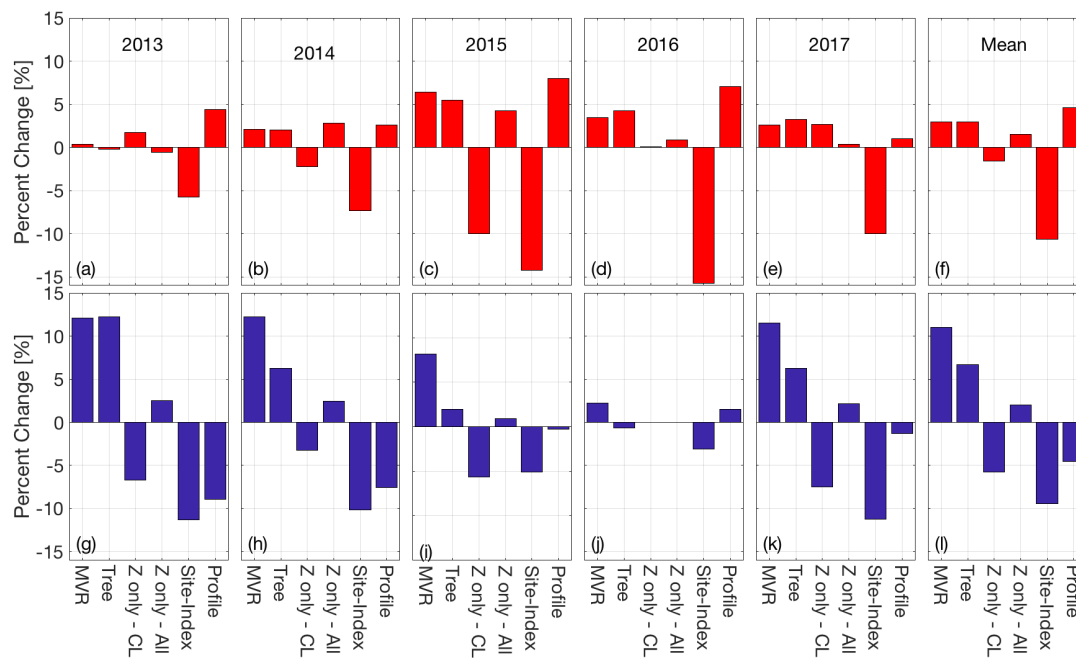
1082 Figure 12. Interannual variability of the SWE accumulation pattern as a function of
1083 cumulative glacier area, shown as (a) normalized range and (b) and r^2 . Solid lines are for
1084 multivariable regression (MVR) and dashed lines are regression tree.
1085



1086
1087
1088
1089
1090
1091
1092
1093
1094
1095
1096
1097
1098
1099
1100



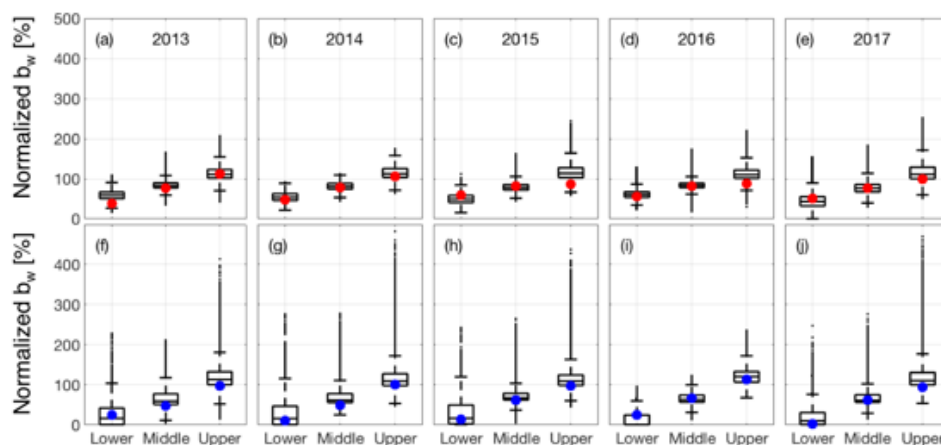
1101 Figure 13. Percent deviation for each estimate from the six-method mean of B_w .
 1102 Individual years for Gulkana Glacier are shown in panels a-e with the five-year
 1103 mean shown in f. Individual years for Wolverine Glacier are shown in panels g-k,
 1104 with the five-year mean shown in l.



1105
 1106
 1107
 1108
 1109
 1110
 1111
 1112
 1113
 1114
 1115
 1116
 1117
 1118
 1119
 1120



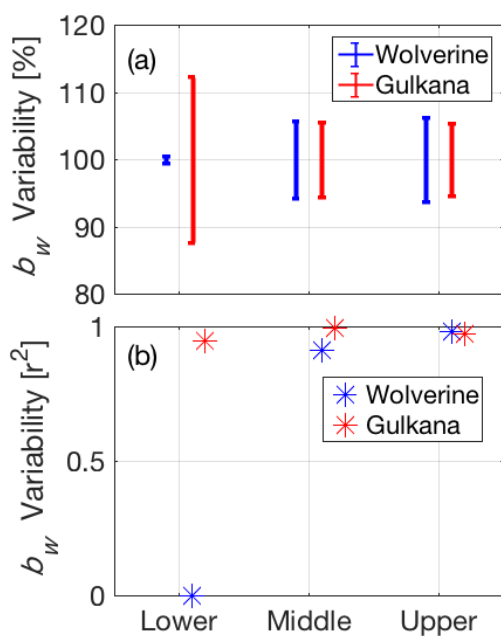
1121 Figure 14. Spatial variability in snow accumulation for individual years (2013-2017) by
1122 elevation (lower, middle, upper) compared to stake measurements. Box plot of all
1123 distributed SWE values (from multivariable regression) for each index zone of the glacier
1124 for Gulkana (a-e) and Wolverine (f-j) for 2013-2017. The filled circles are the respective
1125 stake observation for that index zone. SWE is expressed as a percentage of the glacier-
1126 wide average, B_w , for that year and glacier.



1127
1128
1129
1130
1131
1132
1133
1134
1135
1136
1137
1138
1139
1140
1141
1142
1143
1144
1145
1146



1147 Figure 15. Interannual variability in the spatial pattern of snow accumulation at long-term
1148 mass balance stake locations for Wolverine and Gulkana glaciers using a) normalized b_w
1149 range and b) coefficient of determination (from Figure 11; MVR model).
1150



1151
1152
1153
1154
1155
1156
1157
1158
1159
1160
1161
1162